g- and A-Tensor Calculations in the Zero-Order Approximation for Relativistic Effects of Ni Complexes $Ni(mnt)_2^-$ and $Ni(CO)_3H$ as Model Complexes for the Active Center of [NiFe]-Hydrogenase

Matthias Stein,[†] Erik van Lenthe,[‡] Evert J. Baerends,[‡] and Wolfgang Lubitz*

Max-Volmer-Institut für Biophysikalische Chemie und Biochemie, Technische Universität Berlin, Strasse des 17. Juni 135, D-10623 Berlin, Germany, and Theoretical Chemistry, Vrije Universiteit, De Boelelaan 1083, NL-1081 HV Amsterdam, The Netherlands

Received: July 7, 2000; In Final Form: October 16, 2000

Fully relativistic calculations in the zero-order regular approximation (ZORA) for relativistic effects were performed for the inorganic complexes bis(maleonitriledithiolato)nickelate(III) ($Ni(mnt)_2^-$) and nickeltricarbonylhydride ($Ni(CO)_3H$). They have some similarities with the active center of the [NiFe] hydrogenase. The influence of scalar-relativistic (SR) effects on the structural parameters are discussed. For both complexes, magnetic resonance parameters (**g**-, hyperfine, and quadrupole tensors) are obtained. The deviation of the calculated **g**-tensor values from the experimental data is proportional to the deviation from the free electron value. The agreement between calculated and experimental hyperfine tensors for transition metals is very good when scalar-relativistic (SR) effects and spin−orbit (SO) coupling are considered. The isotropic hyperfine interaction is taken from SR unrestricted calculations and the anisotropic part from SR and SO spin-restricted calculations. The relativistic effects are not so large for the lighter ligand atoms.

1. Introduction

Transition metals are required for many biochemical processes, as catalysis, electron transfer or gene regulation.[1] Consequently, the investigation of biologically essential transition metals is a field of intense research. In recent years, six nickel-containing enzymes were discovered (for a review, see refs 2−5). A prominent example are the [NiFe] hydrogenases.[6,7] Hydrogenases are enzymes that catalyze the reversible oxidation of molecular hydrogen into protons and electrons. Some of the redox states of the enzyme (called Ni−A, Ni−B, and Ni−C) are paramagnetic and can thus be investigated by electron paramagnetic resonance (EPR) spectroscopy. Although the heterobimetallic active center is made up of Ni and Fe, the Fe is EPR-silent ($S = 0$) and the spectrum originates from the Ni atom alone.[8,9] There is considerable interest in understanding the electronic structure of [NiFe] hydrogenases which is available from a combined approach of EPR techniques and theoretical (DFT) calculations. However, before DFT methods can be applied to calculate magnetic resonance parameters of [NiFe] hydrogenase, their accuracy must be evaluated on simple model complexes, which is the aim of this paper.

The biomimetic chemistry of inorganic nickel compounds has been extensively reviewed by Halcrow and Christou.[10]

The choice of the model compounds (Figure 1) containing Ni as the central metal atom was made on the following grounds: in bis(maleonitriledithiolato)nickelate(III) ($Ni(mnt)_2^-$) (**I**) the nickel atom possesses a similar coordination sphere as in [NiFe] hydrogenases. In the hydrogenases, Ni in the active center is coordinated in a distorted tetrahedron sphere by four cysteine amino acid residues.[11,12] In $Ni(mnt)_2^-$, nickel is also bound to four sulfur atoms in a square planar coordination sphere. The Ni(III) oxidation state present in $Ni(mnt)_2^-$ is also discussed for the oxidized forms Ni−A and Ni−B of the [NiFe] hydrogenase. In the neutral complex $Ni(CO)_3H$ (**II**) the nickel is formally in its +1 oxidation state and a hydride ion is axially bound to the Ni. This bonding situation resembles the one discussed for the catalytic intermediate Ni−C of the hydrogenase.[6]

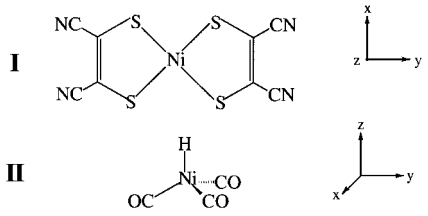

Figure 1. Schematic representation of the investigated nickel complexes bis(maleonitriledithiolato)nickelate(III) $Ni(mnt)_2^-$ (**I**) and nickeltricarbonylhydride $Ni(CO)_3H$ (**II**) with their local coordinate axes systems.

$Ni(mnt)_2^-$ has been very well characterized and the calculations performed on this complex may therefore serve as a benchmark for evaluating the methodology. The **g**-tensor orientation was obtained from single-crystal measurements.[13] From ^{61}Ni enriched single crystals Maki and Edelstein obtained the Ni hyperfine tensor.[13] Furthermore, all ^{33}S hyperfine tensors were determined from angular dependent EPR spectra.[14] Recently, $Ni(mnt)_2^-$ regained interest as model cluster for [NiFe] hydrogenase and, in addition to the existing data, the ligand ^{13}C hyperfine tensor and ^{14}N hyperfine and quadrupole tensors and ^{15}N hyperfine tensor were determined by orientation selected pulsed-ENDOR and ESEEM spectroscopy.[15]

* To whom correspondence should be addressed. Prof. Dr. W. Lubitz, Max-Volmer-Institut für Biophysikalische Chemie und Biochemie, TU Berlin, Sekr. PC14, Strasse des 17. Juni 135, D-10623 Berlin, Germany. Phone: +49-30-314 21419. Fax: +49-30-314 21122. E-mail: lubitz@struktur.chem.tu-berlin.de.

[†] Max-Volmer-Institut für Biophysikalische Chemie und Biochemie.

[‡] Theoretical Chemistry.

10.1021/jp002455g CCC: $20.00
Published on Web 12/19/2000

X_α calculations[16] and recent BLYP calculations[15] only gave atomic spin populations. Very recently, a publication on the DFT calculation of hyperfine tensors of $Ni(mnt)_2^-$ appeared.[17] Discouraging results were obtained from various functionals. The calculated hyperfine tensors were of first-order only and no route of improvement was suggested. There are a number of quantum chemical investigations for the Ni complex with hydrogens replacing the CN groups. They range from Hückel[18] and Pariser−Parr−Pople[19] to Hartree−Fock,[18,20,21] MP2,[22] and DFT calculations.[23] For $Ni(CO)_3H$, there is only one DFT study to our knowledge that aimed to calculate the hyperfine interaction.[24]

Very often, the analysis of experimental hyperfine splittings is limited to the discussion of atomic spin populations. The measured hyperfine couplings are related to theoretical values of singly occupied atomic orbitals[25] and the orbital occupation is obtained as the ratio of experimental to theoretical values. A more direct route to the comparison of experimental and calculated magnetic resonance parameters is given by the *first principles* calculations of the EPR parameters, e.g., as done in this paper from a density functional theory (DFT) wave function. Although the merit of DFT methods in the calculation of hyperfine parameters of organic radicals is unquestionable, its value for the description of paramagnetic resonance parameters of heavier elements, i.e., transition metal complexes, is still largely unexplored.[17] Belanzoni et al. demonstrated the importance of un-freezing core electrons in the calculation of **g**- and **A**-tensors.[26,27] Swann and Westmoreland[28] investigated molybdenum(V) oxyhalide anions using a spin-polarized wave function without un-freezing the core. Schreckenbach and Ziegler[29,30] used a Pauli-type relativistic Hamiltonian with the inclusion of spin−orbit coupling based on second order perturbation theory which was later also applied to study transition metal complexes.[31] Recently, Munzarova and Kaupp critically evaluated the use of various DFT functionals in the calculation of hyperfine parameters of a number of transition metal complexes.[24] They used a nonrelativistic calculation of hyperfine parameters based on geometries that were optimized using a relativistic effective core potential (RECP). However, in this work no **g**-tensors were calculated.

With the zero-order regular approximation (ZORA) for relativistic effects[32,33] one has a fast and powerful tool at hand to calculate the hyperfine tensor **A**, the quadrupole tensor **Q** and the **g**-tensor of systems containing heavy elements.[34,35] Here we apply the ZORA formalism in order to validate its application for the calculation of magnetic resonance parameters for transition metal complexes, in particular [NiFe] hydrogenases. The ZORA formalism seems to overcome the shortcomings of the other approaches used so far. In addition, the influence of scalar-relativistic and variationally spin−orbit coupled DFT wave functions on the **g**- and **A**-tensors for light and heavy elements can be separately studied so that the influence of second-order contributions to the hyperfine coupling can be rationalized. The computational efficiency of the ZORA method makes it an ideal tool for investigating the active centers of metalloenzymes.

2. Computational Details

The calculations reported here are based on the Amsterdam Density Functional program package[36] characterized by Slater-type orbital (STO) basis sets, the use of a density fitting procedure to obtain accurate Coulomb and exchange potentials in each SCF cycle and an accurate and efficient numerical integration of the effective one-electron Hamiltonian matrix elements.[37] All electrons were included in the calculations, there were no frozen core electrons. The ZORA Hamiltonian[32,33] was used for the inclusion of relativistic effects which will be referred to as scalar-relativistic (SR) effects and spin−orbit (SO) coupling. Both are treated variationally. Geometry optimizations were performed at the ZORA SR level for which gradients are available.[38] The **A**-tensors and **g**-tensor are obtained from the ZORA Hamiltonian in the presence of a homogeneous time-independent magnetic field which is then introduced via first-order perturbation theory.[34,35] The **g**-tensor is obtained from a spin-nonpolarized wave function since spin-polarization effects in spin−orbit coupled equations are difficult to calculate, see, e.g., ref 39. The effect of spin-polarization is assumed to be similar to that observed when going from a SR spin-restricted open shell Kohn−Sham (ROKS) calculation to a SR spin-unrestricted open shell Kohn−Sham (UKS) calculation. The **g**-tensor deviates from that of a free electron g_e due to spin−orbit coupling. It is convenient to give the principal values of the **g**-tensor (g_x, g_y, g_z) as the deviation from g_e multiplied by a factor 1000 (in ppt), e.g. $\Delta g_i = (g_i - g_e) \times 1000$, $i = x, y, z$.

The Becke exchange functional[40,41] was used in conjunction with the Perdew correlation functional[42,43] (BP). The BP86 functional has been shown to yield best magnetic resonance parameters of the pure GGA functionals.[27] The basis sets used were relativistic ZORA basis sets from the ADF1999 distribution. Basis set II refers to a double-ζ basis set for light atoms and triple-ζ for first row transition metals. Basis set IV denotes a triple-ζ basis set with one added polarization function for light atoms (C, N, S), basis V has a further polarization function on atoms C, N, S. Basis set V+1s (for Ni and S only) possesses an added tight 1s function in order to improve the description of the wave function near the atomic core. The basis set "Big" denotes a large basis set. This basis set is triple-ζ in the core and quadruple-ζ in the valence with at least three polarization or diffuse functions added.

Calculations for the **g**-tensor were also performed using a traditional second-order perturbation theory (SPT) approach. The spin−orbit coupling constants were calculated from fully relativistic numerical (basis-free) atomic calculations: $\xi(Ni) = 855.4\ cm^{-1}$ and $\xi(S) = 460.4\ cm^{-1}$. For comparison Gaussian94[44] calculations were also performed using the B3LYP hybrid functional with an admixed exact Hartree−Fock (HF) exchange.[45,46] The hyperfine coupling constants in this case are nonrelativistic and of first-order only, following refs 47−49.

3. Results and Discussion

3.1. $Ni(mnt)_2^-$. In the bis(malenonitriledithiolato)-nickelate-(III) complex (**I**, Figure 1) the central nickel atom is coordinated in a square-planar arrangement by four sulfur atoms (point group D_{2h}). From the magnetic resonance studies on single crystals, the orientation of the principal axes of the hyperfine tensor **A** and the **g**-tensor were obtained in a molecule-fixed coordinate system. Maki et al. determined the orientation of the **g**- and ^{61}Ni **A**-tensors in magnetically diluted single crystals of the diamagnetic host $(n\text{-}Bu_4N)_2[Ni(mnt)_2]$.[13] They found that **g**- and ^{61}Ni **A**-tensors are collinear (within experimental error of 2−3°) and that the magnetic axes systems in the crystal are coincident with the symmetry axes of the complex in the crystal. A $(3d_{yz})^1$ electronic configuration was inferred with the *z*-axis perpendicular to the molecular plane and the *y*-axis bisecting each ligand (see Figure 1 top). This assignment was later confirmed by EPR experiments of the ^{33}S enriched complex in single crystals.[14] The ^{33}S hyperfine tensor has axial symmetry within experimental error and the unique axis was found to lie along

TABLE 1: Comparison of Experimental and Calculated Structural Parameters of $Ni(mnt)_2^-$[a]

	X-ray structure[50]	ZORA SR BP/II	ZORA SR BP/IV	ZORA SR BP/V	NR BP/V	NR B3LYP/VTZP
r(Ni−S)	2.15	2.216	2.163	2.156	2.165	2.190
r(S−C)	1.72	1.805	1.737	1.733	1.733	1.747
r(C═C)	1.37	1.381	1.390	1.388	1.389	1.372
r(C−C)	1.44	1.415	1.419	1.417	1.418	1.421
r(C≡N)	1.13	1.181	1.169	1.167	1.168	1.156
∠(S−Ni−S)	92.5	92.58	92.04	91.91	91.70	91.80
∠(Ni−S−C)	103.0	103.39	104.23	104.45	104.43	103.61
∠(S−C═C)	120.0	120.32	119.74	119.59	119.73	120.49
∠(C═C−C)	121.0	122.59	122.75	122.89	122.84	122.44
∠(C−C≡N)	179.0	179.02	178.71	178.77	178.70	178.57

[a] Bond lengths (*r*) in angstroms, bond angles (∠) in degrees.

the molecular *z*-axis. The measured hyperfine tensor is consistent with the **g**-tensor analysis and a $3d_{yz}$ unpaired electron with significant delocalization into sulfur ligand p_z orbitals.[14] Experimental **g**- and hyperfine tensors are given in Tables 2 and 3.

3.1.1. Geometrical Parameters. Table 1 compares calculated structural parameters with averaged experimental data from the X-ray structure analysis.[50] With a small basis set (Basis II) the deviation in bond lengths is 0.07 Å for Ni−S bonds and 0.08 Å for S−C bonds, while bond angles are satisfactorily described. Carbon−carbon single and double bonds as well as C≡N bonds are well described (deviation 0.01 to 0.05 Å). A systematic improvement in bond lengths is obtained when the basis set is enlarged from double-ζ to triple-ζ (basis set II to IV) and when a further set of polarization functions is added (basis set V). The average deviation at the ZORA SR BP/V geometry is 0.02 Å in bond lengths and 0.9° in bond angles and therefore agrees with the X-ray structure analysis within error.

The effect of (scalar)-relativistic effects on the structural parameters of $Ni(mnt)_2^-$ is shown by comparing scalar-relativistic (SR) ZORA and nonrelativistic (NR) geometries. Both calculations used the same functional and basis set. The Ni−S bond lengths are reduced by 0.01 Å when SR effects are included in the ZORA Hamiltonian. The decrease in Ni−S bond lengths causes an increase in the S−Ni−S bond angle from 91.70° to 91.91° when SR effects are considered. All other bond lengths and bond angles remain nearly unaffected upon inclusion of such effects.

For comparison we also include calculations with the B3LYP hybrid-functional. A large Gaussian basis set (GTO) valence-triple-ζ basis set with added polarization functions (VTZP) was used.[51] Hayes[17] very recently reported a UKS B3LYP/6-311+G* geometry optimization of the $Ni(mnt)_2^-$ complex. His findings for the structural parameters are essentially identical to our B3LYP/VTZP results and are therefore not given here. The B3LYP functional proves to be better in the description of bonding parameters of light elements, i.e., the C═C double bond, the C−CN single bond and the C≡N triple bond are slightly more accurately reproduced (by ≈ 0.01 Å) compared to the ZORA SR/V case. Ni−S and S−C bond lengths are, however, too long with the B3LYP functional with respect to the data from X-ray analysis. The hybrid functional also gives slightly better results for bond angles as compared with the X-ray data but the differences between the pure GGA and the hybrid functional are very small (less than 0.8°).

3.1.2. Electronic Structure and g-Tensor Calculations. In the calculations the unpaired electron resides in the $5b_{3g}$ orbital. A Mulliken population analysis of this singly occupied molecular orbital (SOMO) yields only a 21% contribution of the Ni $3d_{yz}$ orbital, 60% S $3p_z$ orbitals, 12% C═C $2p_z$ orbitals and 6% N $2p_z$ orbitals. The exact numbers will depend on the basis set used but the overall picture remains unchanged. The SOMO has a node on the C≡N carbon atom which contributes to less than 1%. The highest fully occupied molecular orbital (HOMO-1) is made up of 62% Ni $3d_{xz}$, 19% S $3p_z$, 11% C $2p_z$ and 5% N $2p_z$. The lowest unoccupied molecular orbital (LUMO) consists of 33% Ni $3d_{xy}$, 32% S $3p_x$ and 22% S $3p_y$. Upon electrochemical two electron reduction, the SOMO would be doubly and the LUMO singly occupied to yield the paramagnetic complex $Ni(mnt)_2^{3-}$.[52]

TABLE 2: Comparison of Calculated and Experimental g-Tensor of $Ni(mnt)_2^-$[a]

	g-value					
	g_x	g_y	g_z	Δg_x[b]	Δg_y[b]	Δg_z[b]
exptl[13]	2.16	2.04	2.00	158	38	−2
exptl[15]	2.14	2.04	1.99	138	38	−12
ZORA SO BP/II	2.102	2.032	1.978	100	30	−24
ZORA SO BP/IV	2.092	2.031	1.976	90	29	−26
ZORA SO BP/V	2.094	2.031	1.976	92	29	−26
ZORA SO BP/V+1s	2.094	2.031	1.976	92	29	−26
ZORA SO BP/Big	2.101	2.033	1.974	99	31	−28
SPT ROKS BP/II	2.123	2.020	1.988	121	18	−14
SPT UKS BP/II	2.105	2.020	1.984	103	18	−18
SPT UKS BP/II ($\xi(S) = 0$)	2.104	2.020	1.984	102	18	−18
SPT UKS BP/II ($\xi(Ni) = 0$)	2.0024	2.0023	2.0023	0.1	0	0

[a] All calculations were performed at the ZORA SR BP/V optimized geometry. The orientation of the **g**-tensor axes is along the symmetry axes of the complex. See Figure 1. [b] Δg_i in ppt.

The *g* values determined by Maki et al.[13] and by Huyett et al.[15] differ in the g_x and g_z values (See Table 2). The deviation along g_x (0.02) and along g_z (0.01) is probably due to crystal packing effects or interaction with the host lattice in the single-crystal experiments[13] or solvent effects in the case of the frozen solution measurements.[15] We tend to favor the *g* principal values from the most recent frozen solution experiments[15] because they provided the basis for the complex analysis and simulation of ENDOR and ESEEM spectra.

Table 2 gives a comparison of experimental and calculated **g**-tensor components for $Ni(mnt)_2^-$. The calculations using the ZORA approach for relativistic effects with inclusion of spin−orbit coupling and a small basis set (basis II) yields *g*-values of 2.102, 2.032, 1.978 for g_x, g_y, and g_z, respectively. The deviation of the calculation is largest for the g_x-component (38 ppt), smallest for g_y (8 ppt), and intermediate for g_z (12 ppt) as compared with the experimental values. The extension of the basis set from a double-ζ to a triple-ζ basis (basis IV) and to one with added polarization functions (basis V) does not improve results but slightly increases the deviation of the calculated **g**-tensor components from the experimental ones. Patchkovskii and Ziegler also observed such an independence of the DFT calculated **g**-tensors from the basis set.[31] Increase of the core region, obtained by adding a further tight 1s function

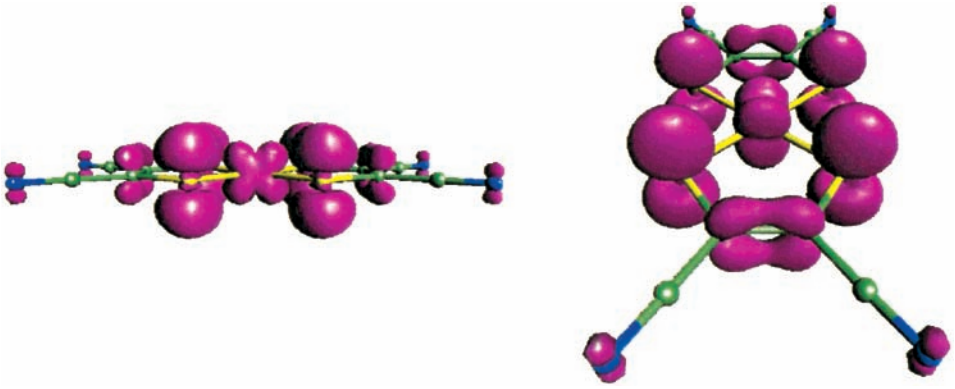

Figure 2. Views of the unpaired spin density distribution of $Ni(mnt)_2^-$ at 0.003 e/a_0^3. The left view is along the *yz*-plane of the complex with the *x*-axis coming out of the paper plane. In the right view the complex is rotated in the plane by 90° and is tilted by approximately 20° out of the plane.

to basis V, does also not improve the **g**-tensor results. This is due to the fact that the **g**-tensor is a property of the valence electrons.[29] All calculated **g**-tensor principal values are systematically smaller than the experimental ones. This is due to the fact that the paramagnetic contribution to the **g**-tensor is too small which is also observed in **g**-tensor calculations of other transition-metal complexes (M. Kaupp, personal communication).

To validate whether the deviations of the calculated **g**-tensors were due to the ZORA approach, a traditional second-order perturbation approach was also used (SPT). A restricted open shell Kohn−Sham calculation in the SPT treatment gives a **g**-tensor with smaller deviation along g_x (17 ppt) and g_z (2 ppt) but larger deviation along g_y (20 ppt). The consideration of spin-polarization effects in the perturbation treatment leads to *g* values of 2.105, 2.020, and 1.984 and, again, comes very close to the ZORA BP/II results. The effect of spin−orbit coupling is incorporated in the second-order perturbation approach and the ZORA formalism. Both give a very similar value for the influence of spin−orbit coupling.[35]

It is known that the deviation of the *g*-value from that of the free electron g_e is determined by spin−orbit coupling which gives the unpaired electron some small angular momentum and thus alters its effective magnetic moment. The SPT methodology offers the opportunity to selectively switch the spin−orbit coupling of different nuclei on or off. The contribution of spin−orbit coupling by the nickel nucleus alone to the **g**-tensor can be obtained by setting the spin−orbit coupling constant of the sulfur nucleus to zero. In the SPT UKS BP/II(ξ(Ni) = 0) calculation only spin−orbit coupling due to the sulfur nuclei is considered. As expected, for g_z and g_y isotropic values of the free electron *g*-factor are obtained. The spin−orbit coupling of the sulfur nuclei only contribute to g_x for which a marginal deviation from g_e (2.0024 vs 2.0023) is obtained. From the comparison of the SPT UKS BP/II(ξ(S) = 0) calculation to the SPT UKS BP/II calculations it is immediately clear that 100% of the g_z- and g_y-values originate from spin−orbit coupling of the nickel atom. The only slight reduction is obtained for g_x (2.105 vs 2.104).

For $Ni(mnt)_2^-$, ZORA calculations with a small basis set already give **g**-tensor magnitude and orientation in satisfying agreement with the experimental values. The agreement cannot be significantly improved by enlarging the basis set. The absolute deviation between calculation and experiment increases with the deviation from the free electron value while the relative error remains about constant. Patchkovskii and Ziegler also observed that the deviation between calculated and experimental **g**-tensors increased when going from 3d to 4d and 5d transition metal complexes.[31] This gives an indication of the accuracy of **g**-tensor calculations one could expect in related work on the active center of [NiFe] hydrogenases. For the oxidized Ni(III) Ni−B EPR spectrum with 2.33, 2.16, 2.01 for g_x, g_y, and g_z, respectively, one might get the largest deviation for g_x (if the error is strictly proportional to the deviation from g_e one would expect a deviation of up to 0.1) and better agreement for the g_y and g_z components. Furthermore, for the comparison of "gas phase" **g**-tensor calculations and experiments in single crystals an agreement of 10−15% would already be considered satisfying.[24]

3.1.3. Spin Density Distribution and Hyperfine Interactions. Figure 2 shows contour plots of the unpaired spin density at $0.003e/a_0^3$. The spin density is not fully localized at the central nickel atom, but the four surrounding sulfur atoms carry significant spin density in p_π lobes oriented perpendicular to the horizontal mirror plane. The carbon atoms of the carbon−carbon double bond also bear unpaired spin density in their π-bonds. In contrast, the carbon atoms of the cyanide group carry no unpaired spin density while the terminal nitrogen atoms exhibit a small lobe of unpaired spin in a p-orbital perpendicular to the plane of the molecule.

Unrestricted ZORA SR BP/V calculations yield total atomic spin populations of 0.26 at the nickel atom, 0.16 at each sulfur atom, 0.02 at each carbon in the double bond, −0.003 at each carbon of the cyanide group and 0.01 at each N. The $Ni-S_4$ core thus bears 90% of the unpaired spin. This value is slightly larger than the one from BLYP/LANLDZ results by Huyett et al.,[15] who found 75%, and is close to X_α[16] calculations where 82% were found. In the non- and scalar-relativistic calculations one may discuss atomic spin densities as the difference between α and β atomic electron densities. In relativistic calculations, where spin−orbit coupling requires spin mixing, the resulting SO-coupled states will no longer be pure spin states. This will complicate the interpretation in terms of atomic spin densities.[39]

The high covalency of Ni−S bonds and the significant delocalization of spin density into ligand orbitals might have a significant influence on the interpretation of EPR and ENDOR spectra of biological Ni−S centers, for instance in the case of [NiFe] hydrogenase for which large isotropic ^1H hyperfine coupling constants were measured for β-CH_2 protons of a cysteine amino acid adjacent to a nickel atom.[53]

The single-crystal experiments by Maki et al.[13] yielded the ^{61}Ni hyperfine tensor. It was found to be collinear with the **g**-tensor principal axes within experimental error. Unfortunately. the signs of the principal hyperfine tensor components (A_{xx} = 45 ± 6 MHz, A_{yy} = 9 ± 3 MHz, A_{zz} = <6 MHz) are not known. The measured hyperfine interaction in liquid solution is a_{iso} =

TABLE 3: Experimental and Calculated Hyperfine and Quadrupole Parameters of $Ni(mnt)_2^-$ in MHz

nucleus	hf component[a]	exptl	SR ROKS BP/V+1s	SR UKS BP/V+1s	SO + SR ROKS BP/V+1s	UKS B3LYP VTZP
^{61}Ni[b]	a_{iso}	+18	−0.12	+18.60	−15.03	+30.82
	A'_{xx}	+27	+47.15	+51.93	+25.87	+66.92
	A'_{yy}	−9	−23.53	−24.03	−7.88	−28.52
	A'_{zz}	−18	−23.85	−27.35	−17.99	−38.40
^{33}S[c]	a_{iso}	+5.2	+0.12	+3.11	+0.19	+7.20
	A'_{xx}	−18.8	−13.49	−15.79	−13.81	−18.46
	A'_{yy}	−18.8	−13.15	−14.38	−12.65	−15.32
	A'_{zz}	+37.6	+26.65	+30.16	+26.45	+33.77
$^{13}C{=}C$[d]	a_{iso}	−2.1	+0.003	−1.63	+0.11	−2.32
	A'_{xx}	−2.5	−3.49	−2.95	−3.09	−2.09
	A'_{yy}	−2.5	−3.15	−2.63	−3.26	−1.49
	A'_{zz}	+5.0	+6.65	+5.59	+6.37	+3.58
^{13}CN[d]	a_{iso}	−2.9	−0.001	−2.47	+0.01	−1.95
	A'_{xx}	+0.33	−0.31	−0.25	−0.51	−0.50
	A'_{yy}	+0.13	+0.81	+0.80	+0.83	+0.62
	A'_{zz}	−0.47	−0.50	−0.54	−0.31	−0.12
^{14}N[d]	a_{iso}	+0.39	+0.001	+0.15	+0.007	+0.15
	A'_{xx}	−0.26	−0.72	−0.59	−0.73	−0.40
	A'_{yy}	−0.29	−0.60	−0.47	−0.59	−0.22
	A'_{zz}	+0.55	+1.33	+1.05	+1.31	+0.62
	Q_{xx}	+0.85	+0.86	+0.85	+0.86	+0.41
	Q_{yy}	+1.10	+1.23	+1.23	+1.23	+1.80
	Q_{zz}	−1.95	−2.09	−2.09	−2.09	−2.21

[a] a_{iso} is the isotropic (Fermi contact) hyperfine interaction; A'_{ii}, $i = x, y, z$, are the anisotropic hyperfine tensor components. (b) Only Choice I of the signs of the experimental hyperfine tensor components is given (see text for details) exptl values from ref 13. (c) Only Choice II of the experimental hyperfine tensor components is given (see text for details) exptl from ref 14. (d) The absolute signs of the experimental tensors were fixed by assuming spin density in the $2p_z$ orbital (see ref 15), exptl from ref 15.

12.6 ± 2.8 MHz. If one assumes that the A_{zz} component is zero, one only arrives at two possibilities: Choice I, where all tensor components are positive: $A_{xx,yy,zz} = (+45, +9, 0)$ MHz yields $a_{iso} = +18$ MHz and for the purely anisotropic components $A'_{xx,yy,zz} = (+27, -9, -18)$ MHz. (Choice II) $A_{xx,yy,zz} = (+45, -9, 0)$ yields $a_{iso} = +12$ MHz, $A'_{xx,yy,zz} = (+33, -21, -12)$ MHz. Estimates where A_{zz} is small but not zero, do not basically change the discussion of the results.[54] A discrimination between the two combinations can be done on the basis of calculations of the (anisotropic) ^{61}Ni hyperfine interaction (see Table 3).

The analysis of naturally abundant ^{33}S satellites yielded an axial ^{33}S hyperfine tensor ($A_{zz} = A_{||} = 42.8$ MHz, $A_{xx} = A_{yy} = A_{\perp} = 13.6$ MHz). Two choices of the signs of the hyperfine tensor were discussed in ref 14. (I) All signs are positive, the isotropic value is 23.3 MHz, and the anisotropic values $A'_{xx,yy,zz} = (-9.7, -9.7, 19.5)$ MHz. (II) When $A_{\perp} = A_{xx} = A_{yy}$ values are negative, then the isotropic coupling is 5.2 MHz and the anisotropic hyperfine tensor $A'_{xx,yy,zz} = (-18.8, -18.8, 37.6)$ MHz. The atomic spin population at the sulfur was estimated from the uniaxial hyperfine tensor and using the theoretical atomic values of Morton and Preston[25] to be between 0.13 ($A_{||}$ and $A_{\perp}$ same sign) and 0.26 ($A_{||}$ and $A_{\perp}$ opposite signs).[14] This agrees with the picture in which a $3p_z$ orbital occupation induces a polarization of the Ni−S σ orbitals. From this, one expects a small isotropic hyperfine interaction. The larger value of 23.3 MHz, however, appears unrealistic.

Table 3 shows a comparison of experimental and calculated hyperfine tensors of $Ni(mnt)_2^-$. For the experimental ^{61}Ni and ^{33}S hyperfine interactions a plausible choice of signs of the hyperfine tensor components was made (see above). In the case of ^{13}C and ^{14}N nuclei the choice of hyperfine tensor signs from ref 15 is given (which proved to be in agreement with the calculations). All calculations were done at the unrestricted SR ZORA BP/V geometry (see Table 1). For means of comparison we also performed a spin-unrestricted B3LYP calculation with a valence-triple-ζ basis set with polarization functions given by Schäfer et al.[15]

SR ROKS calculations yield reliable anisotropic hyperfine tensors while the isotropic hyperfine interaction is not trustworthy since the effect of spin-polarization is not considered. For ^{61}Ni, the calculated anisotropic hyperfine tensor deviates by a factor of 2 for the anisotropic hyperfine tensor components A'_{xx}, A'_{yy}. The agreement for A'_{zz} is better. Spin-polarized ZORA SR calculations (SR UKS) yield an isotropic hyperfine interaction of +18.60 MHz for ^{61}Ni which nicely corresponds to an experimental value of +18 MHz (Choice I). The effect of spin-polarization on the anisotropic hyperfine tensor components is less pronounced. A'_{xx} and A'_{zz} are increased by approximately 4 MHz in absolute numbers upon consideration of polarization effects, whereas the effect on A'_{yy} is very small. Still, the agreement with experimental data is far from satisfying. Nonrelativistic UKS B3LYP calculations with a VTZP basis set give similar numbers but the agreement with experimental data is even worse. This obvious discrepancy which was also observed by Hayes[17] led the author to the pessimistic conclusion that density functional calculations on $Ni(mnt)_2^-$ are unable to reliably assign the signs of the ^{61}Ni hyperfine tensor. The disagreement with experimental data, however, is not due to deficiencies of either the basis set or the functional but due to a systematic neglect of spin−orbit coupling as shown below.

The spin−orbit coupling manifests itself as a pseudocontact contribution to a_{iso} and a second-order contribution to the anisotropic hyperfine tensor.[26,55−58] The effect of spin−orbit coupling is very large for nickel. The inclusion of spin−orbit coupling even inverts the sign of the a_{iso} (Table 3). It must be kept in mind that a considerable part of this difference is due to the neglect of spin-polarization in the spin−orbit coupled equations. A better estimate of the effect of spin−orbit coupling can be made if the spin-restricted SR results and those including spin−orbit coupling are compared. This gives an effect of spin−orbit coupling of approximately 15 MHz. When isotropic hyperfine interactions are to be calculated one still has to resort to spin-polarized (UKS) SR ZORA values until spin-polarized

spin−orbit coupling can be treated in the ZORA Hamiltonian. This work is in progress.

The influence of SO coupling on the anisotropic hyperfine tensor (second order contribution) can, however, very accurately be calculated in the ZORA approach. The absolute signs of the anisotropic hyperfine interaction are retained upon inclusion of spin−orbit coupling but their magnitude is decreased by 22, 16, and 6 MHz for A'_{xx}, A'_{yy}, and A'_{zz}, respectively when comparing SR ROKS and SR+SO ROKS calculations. The lower hyperfine values agree to within one megahertz with the experimental ones of Choice I.

The other choice (Choice II) of the signs of the experimental ^{61}Ni hyperfine tensor can therefore be ruled out on the basis of our ZORA calculations. Neither isotropic (from the spin-polarized SR ZORA calculation) nor SO-coupled anisotropic hyperfine tensors support this possibility.

Our findings indicate that the inclusion of spin−orbit coupling is an absolute necessity when trying to calculate the hyperfine interaction of a transition metal ion. The influence of SO coupling on the anisotropic ^{61}Ni hyperfine interaction reduces it by a factor of 2 and brings it to within excellent agreement with experimental values.

For the ^{33}S hyperfine interaction in $Ni(mnt)_2^-$, the effect of spin−orbit coupling is less pronounced than for the ^{61}Ni nucleus but still noticeable. ZORA SR UKS calculations give an isotropic hyperfine interaction of +3.11 MHz which corresponds to the choice of experimental signs II ($a_{iso} = +5.2$ MHz). Choice I would lead to an unrealistic high value of +23.3 MHz which can also not be reproduced by the calculations. Furthermore, the calculated hyperfine interaction of (−15.79,−14.38,+30.16) MHz supports choice II whereas the anisotropic hyperfine tensor components of choice I appear too low. The effect of spin-polarization becomes obvious when comparing restricted (ROKS) and unrestricted (UKS) open shell SR ZORA calculations. Spin-polarization leads to an increase of A'_{xx}, A'_{yy}, and A'_{zz} in absolute magnitude by 2.3, 1.2, and 3.5 MHz, respectively. The agreement with the experimental values is improved. ZORA calculations with spin−orbit coupling yield an a_{iso} value of only 0.19 MHz. The anisotropic hyperfine tensor does not change much upon inclusion of spin−orbit coupling (changes lie within 0.5 MHz). If the effect of spin-polarization is taken from the SR calculations, values to within 0.5 MHz of the SR UKS can be estimated. The isotropic hyperfine interaction of ^{33}S is due to spin polarization and yields a small but detectable isotropic hyperfine interaction.

For the ^{13}C hyperfine interaction in the C=C double bond, ZORA SR UKS calculations yield isotropic and anisotropic hyperfine interactions to within 0.5 MHz of the experimental ones. The importance of spin polarization again is illustrated by comparing restricted and unrestricted SR calculations. Spin polarization reduces the anisotropic hyperfine tensor components by 0.5−1 MHz and brings them closer to the experimental values. When the effect of spin-polarization is taken from SR calculations the results with SO coupling represent an improvement of 0.4 MHz. B3LYP calculations give good results for the ^{13}C isotropic hyperfine interaction but the anisotropic part is less well reproduced (see also 17). The experimental ^{13}C hyperfine tensor was assumed to be collinear with the **g**-tensor principal axes system. Only in this coordinate system the tensor is of uniaxial symmetry. The deviation of the calculated anisotropic hyperfine tensor from uniaxiality is indeed small. The orientation, however, is not collinear with the **g**-tensor principal axes system but rotated by 6° from the *x*- and *y*-axes. A'_{zz} is along the g_z-axis. This was also noticed by Hayes.[17]

The case of the ^{13}C nucleus of the cyanide group is more difficult. The negative isotropic hyperfine interaction is well reproduced by unrestricted calculations (−2.47 MHz calculated vs −2.9 MHz experimental). All theoretical calculations, however, agree that A'_{xx} is negative and A'_{yy} positive while the simulation of the experimental spectra yielded A'_{xx} and A'_{yy} both of positive sign. Theory and experiment agree that the component perpendicular to the molecular plane, A'_{zz}, is negative. One must bear in mind that the experimental values give the hyperfine tensor in the **g**-tensor's principal axes system, i.e., **g**- and **A** are assumed to be collinear. The calculations yield the diagonalized hyperfine tensor in its own principal axes system which is not necessarily collinear with the **g**-tensor. In fact, A'_{xx} and A'_{yy} are rotated by 30° from the respective **g**-tensor principal axes and A'_{zz} is along g_z (similar values were obtained by Hayes[17]).

For the ^{14}N hyperfine interactions of the CN group spin-polarized (UKS) ZORA SR calculations give excellent results. The deviation from the experimental values is less than 0.5 MHz for both isotropic and anisotropic contributions. B3LYP calculations give slightly better values for the anisotropic hyperfine interaction of the ^{14}N nucleus. The deviation from experimental values might be due to environmental effects in frozen solution. The numbers given in ref 17 for the experiment from ref 15 correspond to the experimental values for the ^{15}N nucleus and have to be corrected by the ratio of the ^{15}N and ^{14}N Larmor frequencies (1.403). For a cyanide group one expects a nearly axial quadrupole tensor with its largest component along the C≡N triple bond. The calculated ^{14}N ($I = 1$) quadrupole tensor agrees well with the experimental values. The calculated quadrupole tensor has its smallest component perpendicular to the molecular plane (0.85 MHz) and its largest component (−2.09 MHz) along the C≡N triple bond. The third component (1.23 MHz) lies in the molecular plane and is perpendicular to the C≡N bond. This orientation was also found experimentally by Huyett et al.[15] The thorough analysis of pulsed-ENDOR and ESEEM data by simulation of the experimental spectra and the assignment of absolute signs[15] of the hyperfine tensors is confirmed by our calculations.

For means of comparison, we also performed a calculation using the popular B3LYP functional and a valence-triple-ζ basis set with polarization functions (VTZP) of Schäfer et al.[51] The geometry of the ZORA SR UKS BP/V (Table 1) calculation was used. The hyperfine interactions were calculated using a nonrelativistic, first-order approach (see for example[47−49]). Strictly speaking, the comparison can only be made with spin-polarized scalar-relativistic ZORA calculations where spin−orbit coupling is not considered. The isotropic ^{61}Ni hyperfine interaction is of positive sign and significantly larger than the ZORA SR value. This may be due to the different density functionals and basis sets used in the calculations. Gaussian basis functions do not correctly describe the cusp region near the core in contrast to the use of Slater basis functions in ADF, which means that one needs to use more GTOs than STOs in the basis set to obtain the same accuracy.[63] The signs of the anisotropic hyperfine tensor components are reproduced in the B3LYP calculations but the values are larger than the corresponding ZORA values. This deficiency is due to the neglect of spin−orbit coupling as we have shown above. For all other nuclei, the absolute signs of the tensor components agree with the ZORA results. The agreement is of the order of a few MHz or less but the B3LYP functional does not represent a systematic improvement over the pure GGA functional. This observation was also made by Munzarova and Kaupp who compared all

TABLE 4: Comparison of Calculated Structural Parameters of $Ni(CO)_3H$[a]

	ZORA SR ROKS BP/V	ZORA SR UKS BP/V	NR UKS BP/V	B3LYP/ RECP(Ni)[24]
r(Ni−H)	1.485	1.495	1.502	1.512
r(Ni−C)	1.807	1.807	1.824	1.851
r(C═O)	1.150	1.149	1.150	1.135
∠(H−Ni−C)	90.87	90.93	89.90	90.87
∠(Ni−C═O)	173.19	173.79	172.38	171.29

[a] Bond lengths in angstroms, bond angles in degree.

usual GGA and hybrid functionals in the calculation of transition metal hyperfine interactions.[24]

To summarize, ZORA calculations yield hyperfine parameters for all (light and heavy) atoms in $Ni(mnt)_2^-$ in good agreement with experimental values. The ambiguity of the signs of the ^{33}S and ^{61}Ni hyperfine tensors could be resolved resulting in one specific choice of signs of the hyperfine tensor components. Spin−orbit coupling plays an important role in the calculation of heavy element anisotropic hyperfine interaction. The isotropic hyperfine interaction must still be taken from a spin-polarized SR ZORA calculation.

In the oxidized states of the [NiFe] hydrogenase, the EPR signal also originates from the Ni metal alone as was shown by ^{61}Ni enrichment.[8] The Fe metal in the active center does not contribute to the EPR spectrum. The hyperfine interaction of the ^{61}Ni enriched hydrogenase from *Desulfovibrio gigas* in the oxidized Ni−B state shows a hyperfine splitting of 6 to 17, 6 to 17, and 76 MHz along the **g**-tensor components g_{xx}, g_{yy}, and g_{zz}, respectively.[59] The hyperfine interaction is therefore of the same order of magnitude as in $Ni(mnt)_2^-$ and we may expect the spin population at the Ni nucleus in [NiFe] hydrogenase to be similar to that in this model complex $Ni(mnt)_2^-$.

3.2. $Ni(CO)_3H$. In $Ni(CO)_3H$ (**II**, see Figure 1) the central nickel atom is coordinated by three CO ligands in the equatorial plane and axially by a hydrogen atom (C_{3v} symmetry). Formally, the complex may be described either as a Ni(I) with a H^- bound ($(CO)_3$−Ni(I)-H^-) or as a Ni(0) with a hydrogen atom bound ($(CO)_3$ −Ni(0)−H). In the thorough analysis of the krypton matrix EPR spectrum, Morton and Preston concluded that the structure of the complex is best described as $(CO)_3$−Ni(I)−H^-.[60] While the oxidized states of the hydrogenase are usually referred to as Ni(III), the two electron more reduced form Ni−C might be a Ni(I) species. Since Ni−C is an intermediate in the catalytic process, either a H_2 molecule, or a H^+ or H^- are supposed to be bound to the Ni. $Ni(CO)_3H$ therefore represents a good model for the calculation of the magnetic resonance parameters for such a bonding situation.

For $Ni(CO)_3H$ there is no X-ray structure available. The comparison of calculated structural parameters is therefore made with DFT calculations by Munzarova and Kaupp[24] who used the B3LYP functional with a relativistic pseudopotential for Ni.

Table 4 compares the calculated structural parameters of $Ni(CO)_3H$ in the ZORA approach at the scalar-relativistic (SR) level using a large basis set (basis V) with those using a relativistic effective core potential (RECP)[24] and non-relativistic all electron calculations. NR calculations agree well with the B3LYP/RECP(Ni) calculations in the Ni−H bond length (1.502 vs 1.512 Å). The Ni−C bond length is shorter by 0.027 Å in the NR calculation and so is the C═O bond length by 0.015 Å. The difference in bond angles is only ≈1°. The influence of scalar-relativistic effects can be observed by comparing non-relativistic ADF calculations with SR ZORA calculations. They are manifested in a reduction of the Ni−H bond length by 0.007 Å and of the Ni−C bond length by 0.017 Å. The effect on the C═O bond length is almost negligible. Because of the shorter Ni−H and Ni−C bonds, the H−Ni−C and Ni−C═O bond angles widen by 0.4°. The importance of spin-polarization for structural parameters is highlighted by comparing restricted open shell Kohn−Sham and unrestricted Kohn−Sham scalar-relativistic ZORA calculations (Table 4). Spin-polarization leads to an increase in Ni−H bond length by 0.01 Å while all other structural parameters remain nearly unchanged. In general, SR UKS ZORA calculations agree well with those using the B3LYP functional and a relativistic core potential. Spin-polarization is important for the description of the Ni−H bond.

TABLE 5: Comparison of ZORA Calculated and Experimental g-Tensor of $Ni(CO)_3H$[a]

	g-value			
	$g_\perp$	$g_\parallel$	$\Delta g_\perp$[b]	$\Delta g_\parallel$[b]
exptl [60]	2.0674	2.0042	65	2
BP/II	2.0468	2.0003	45	−2
BP/IV	2.0478	2.0003	46	−2
BP/V	2.0480	2.0003	46	−2
BP/V+1s	2.0486	2.0003	46	−2

[a] All calculations were performed at the ZORA SR UKS BP/V optimized geometry. The orientation of the **g**-tensor axes is along the symmetry axes of the complex. See Figure 1. [b] Δg_i in ppt.

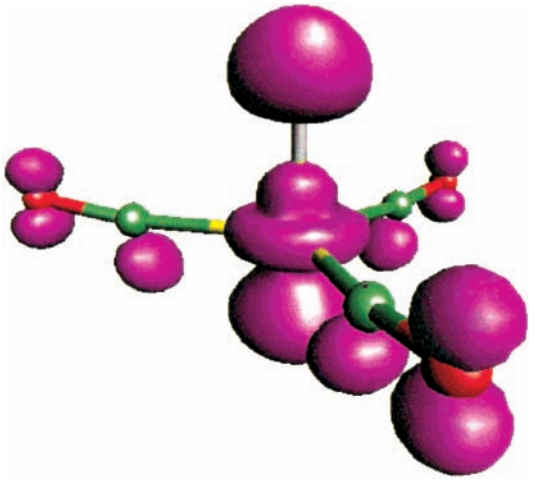

Figure 3. View of the Unpaired Spin Density Distribution of $Ni(CO)_3H$ at 0.003 e/a_0^3.

3.2.1. g-Tensor and Hyperfine Interaction. The EPR spectrum of $Ni(CO)_3H$ was measured in a krypton matrix by Morton and Preston.[60] They found an axial **g**-tensor with $g_\parallel = g_{zz} = 2.0674$ and $g_\perp = g_{xx} = g_{yy} = 2.0042$. The orientation of the **g**-tensor is $g_\parallel$ along the *z*-axis and $g_\perp$ in the *xy* plane of the complex (see Figure 1).

Table 5 gives the results of ZORA calculations of the **g**-tensor of $Ni(CO)_3H$. All calculated values are smaller than the corresponding experimental values. For the small double-ζ basis (basis set II), the deviation of the $g_\parallel$ component is 4 ppt from the experimental value and for $g_\perp$ it is 20 ppt. A better description of the valence electrons does not significantly improve the results. The increase is only 1 ppt in $g_\perp$. The addition of an extra tight 1s function also only marginally improves the results.

Figure 3 shows a contour plot of the unpaired spin density at a value of 0.003 e/a_0^3. The contour plot shows that the spin density distribution is of centroid symmetry. The form of the spin density at the Ni resembles that of a d_{z^2} orbital. A Mulliken analysis yields atomic spin populations of ρ(Ni) 0.48, ρ(H) 0.22,

TABLE 6: Comparison of Experimental and Calculated Hyperfine and Quadrupole Interactions in $Ni(CO)_3H$ in MHz[a]

nucleus	hf component	exptl[60]	SR ROKS BP/V+1s	SR UKS BP/V+1s	SR + SO ROKS BP/V+1s	B3LYP/ DZPD(Ni) IGLO-III[24]
^{61}Ni	a_{iso}	+9.0	−9.94	+10.10	−18.70	+33.3
	$A'_{\perp}$	+44.0	+50.88	+48.56	+45.76	+56.9
	$A'_{\parallel}$	−88.0	−101.75	−97.11	−91.52	−113.8
	$Q_{\perp}$	−4.1	−4.4	−4.1	−4.4	
	$Q_{\parallel}$	+8.2	+8.8	+8.2	+8.8	
^{1}H	a_{iso}	+292.8	+276.54	+335.58	+275.25	+208.0
	$A'_{\perp}$	−5.50	−4.05	−2.68	−4.21	−3.15
	$A'_{\parallel}$	+11.10	+8.11	+5.36	+8.44	+6.30
^{13}C	a_{iso}		+20.75	+7.61	+20.74	+5.10
	A'_{xx}		−5.46	−5.71	−5.59	−5.50
	A'_{yy}		−1.34	−2.60	−1.19	−3.20
	A'_{zz}		+6.80	+8.31	+6.79	+8.70
^{17}O	a_{iso}		−1.31	−3.72	−1.35	−3.70
	A'_{xx}		+7.92	+8.60	+8.00	−8.70
	A'_{yy}		+6.98	+6.99	+6.83	−5.30
	A'_{zz}		−14.90	−15.59	−14.83	+14.0

[a] Calculations were performed at the ZORA SR UKS BP/V geometry (see Table 4).

ρ(C) 0.06, and ρ(O) 0.04. The contribution of the atomic orbitals to the $13A_1$ SOMO are as follows (arranged by decreasing percentage): 24% $3d_{z^2}$ (Ni), 21% $4p_z$ (Ni), 19% $2p_z$ (C), 17% 1s (H), 14% $2p_z$ (O), and 4% 2s (C). This indicates that the $4p_z$ of the Ni contributes significantly.

Because of the axial bonding of the hydride ion to the Ni atom, the H atom may acquire a significant amount of spin density which leads to a very large hyperfine coupling caused by the large magnetic moment of the nucleus. Consequently, the ^{1}H hyperfine structure could be resolved in the Kr matrix EPR spectra.[60] The hyperfine interaction is dominated by a very large isotropic hyperfine interaction a_{iso} of 293 MHz while the uniaxial anisotropic interaction is only 5.5 MHz.

Table 6 compares the ^{61}Ni and ^{1}H experimental hyperfine interactions with ZORA calculations at various levels of theory and non-relativistic B3LYP calculations by Munzarova and Kaupp.[24] The comparison is only made with the results using the B3LYP functional because it is the one most frequently used in DFT investigations of transition metals. The ZORA SR UKS BP/V optimized geometry of Table 4 was used.

The ^{61}Ni isotropic hyperfine interaction is well reproduced by unrestricted (UKS) SR ZORA calculations whereas the B3LYP functional overestimates the isotropic coupling constant by a factor of 3. The inclusion of spin-polarization reduces $A'_{\perp}$ and $A'_{\parallel}$ by 2 and 4 MHz indicating only a moderate effect of polarization. SO coupling reduces the anisotropic coupling by 5 and 10 MHz for $A'_{\perp}$ and $A'_{\parallel}$, respectively, when comparing SR ROKS and SO+SR ROKS calculations. The effect is weaker than in the case of $Ni(mnt)_2^-$ because the SOMO consists here of p_z and d_{z^2} orbitals at the Ni. If the assumption of similar spin-polarization for SR and SO-coupled calculations holds, the agreement with the experimental values is perfect. $A'_{\perp}$ would be brought down to 44 MHz and $A'_{\parallel}$ to 88 MHz by spin-polarization. The resulting anisotropic tensor is in excellent agreement with the experimental value and superior to the B3LYP results by Munzarova and Kaupp.[24] (The BP86 values by Munzarova and Kaupp[24] are in close agreement with our values. Still, the isotropic coupling constant is overestimated by a factor of 2.) The ZORA calculated isotropic hyperfine interaction of the Ni changes from +10.10 to −18.70 MHz upon inclusion of spin−orbit coupling and neglecting spin-polarization. This large effect of −28.8 MHz agrees very well with the estimated value of spin−orbit coupling by Munzarova and Kaupp[24] who used an empirical formula by Abragam and Pryce (see ref 58) and obtained −26.8 MHz. We agree with these authors that this effect is overestimated, since in our calculation the effect of spin-polarization is also neglected. A comparison of the SR ROKS results with the SR UKS results shows that spin-polarization effects already explain for a large part the calculated difference.

Because of the cylindrical spin density distribution (see Figure 3) one expects the largest quadrupole interaction of the ^{61}Ni nucleus ($I = 3/2$) to be along the Ni−H bond and smaller values perpendicular to it. This is found experimentally: $Q_{\parallel} = 8.2$ MHz and $Q_{\perp} = -4.1$ MHz. These numbers are exactly obtained from a spin-polarized SR calculation while non-polarized calculations slightly overestimate the parallel value and underestimate the perpendicular value.

The ^{1}H isotropic hyperfine interaction is overestimated by SR UKS calculations by 43 MHz and also the anisotropic part is not very well described (deviation 3 and 6 MHz). It is in particular the isotropic component that is most sensitive to spin polarization. The calculated B3LYP ^{1}H value by Munzarova and Kaupp[24] deviates from the experimental value by 85 MHz but into the other direction (208 MHz calculated vs 293 MHz measured). A comparison of the spin-restricted (ROKS) SR results and those including spin−orbit (SR+SO ROKS) coupling shows that the effect of spin−orbit coupling is small for the ^{1}H nucleus.

For the ^{13}C and ^{17}O nuclei there are no experimental values available. Here, a comparison is made with the B3LYP calculated values by Munzarova and Kaupp[24] which are also included in Table 6. For the ^{13}C nucleus the agreement between SR UKS ZORA and non-relativistic B3LYP calculations is very good. The difference in the isotropic hyperfine interaction is 2.5 MHz at most. In the case of ^{17}O, in contrast, the SR UKS calculated signs of the anisotropic hyperfine interaction are inverted with respect to the values by Munzarova and Kaupp (see Table 6). We therefore repeated the calculation using the SR ZORA BP/V geometry, a VTZP basis set by Schäfer et al.[51] and the B3LYP hybrid functional in the Gaussian94 program. The obtained values are, in general, very similar to those of Munzarova and Kaupp and are therefore not given here. The only noteworthy difference is in the ^{17}O hyperfine interaction. The isotropic part in our calculation is $a_{iso} = -4.35$ MHz and the anisotropic part $A'_{xx,yy,zz} = (+9.64, +6.11, -15.75)$ MHz. Our findings of the absolute signs of the anisotropic hyperfine interaction are in agreement with our ZORA results and contradict the signs given by Munzarova and Kaupp. We believe this to be a typing error in their manuscript. The effect of spin−orbit coupling is very small for ligands in the molecular *xy*-plane. The anisotropic part of the hyperfine tensor of the ^{13}C and ^{17}O nuclei remains nearly unchanged upon inclusion of SO coupling.

It should be mentioned as an aside that the popular B3LYP functional does not necessarily lead to an improvement in the calculation of hyperfine parameters compared to pure GGA functionals as was already stated by Munzarova and Kaupp[24] and by Hayes.[17]

The Ni−C state of the [NiFe] hydrogenase is two electrons more reduced than the oxidized states, and might formally correspond to a Ni(I) species. The observation of the Ni−C EPR spectrum correlates with the catalytic activity of the enzyme[59] and is thus assigned to be an intermediate in the heterolytic cleavage of molecular hydrogen. For the Ni(I) in Ni−C a $3d_{z^2}$ ground state is sometimes discussed.[2,61,62] As we

have shown here, a hydride axially bound to a Ni $3d_{z^2}$ orbital would lead to a much larger ^{1}H hyperfine coupling than the one observed in hydrogenase (16−20 MHz[61,62]). Such a bonding situation seems therefore to be unrealistic in the Ni−C state.[6] A hydride ion bound to nickel in the *xy*-plane can, however, not be excluded.

4. Conclusion

The calculation of magnetic resonance parameters from first principles offers a straightforward route to the comparison of experimental and theoretical values for transition metal complexes. The detour via atomic spin populations is no longer required.

We have demonstrated the accuracy of the ZORA formalism to calculate the magnetic resonance parameters of nickel containing model complexes both in the formal Ni(III) and Ni(I) oxidation states. The hyperfine tensors can be computed relatively accurately, whereas the agreement in **g**-tensors is less good. Effects of spin−orbit coupling may be large for both the calculated isotropic and the calculated anisotropic metal hyperfine interactions. The effects on the ligand hyperfine interactions are in general much smaller.

In the case of $Ni(mnt)_2^-$, the calculations helped to resolve ambiguities in the choice of signs of the ^{61}Ni and ^{33}S hyperfine couplings. The unpaired electron was found to reside in the $5b_{3g}$ orbital consisting mainly of the Ni $3d_{yz}$ orbital and S $3p_z$ orbitals. The covalent bonding leads to a delocalization of 64% of the spin population into sulfur ligand orbitals. This large Ni−S bond covalency is an important result and has to be taken into consideration in the interpretation and analysis of ENDOR data from the [NiFe] hydrogenases.

In $Ni(CO)_3H$, a hydride ion is bound axially to a hybrid Ni $3d_{z^2}$, $4p_z$ orbital. The large hyperfine interaction of the hydrogen rules out such a bonding situation for the Ni−C state of the [NiFe] hydrogenase. An in-plane bound hydride can, however, not be excluded.

The ZORA formalism's accuracy and computational efficiency holds great promise for the elucidation and interpretation of EPR and ENDOR data of Ni complexes in biological systems and other active centers in metalloenzymes. Calculations are in progress for the various states of the [NiFe] hydrogenase for which extensive experimental data have recently become available.[53,64] In future work, we plan to extend the ZORA methodology to also take spin-polarization into account in spin−orbit coupled DFT calculation.

Acknowledgment. Prof. Brian M. Hoffman (Northwestern University) and Prof. Martin Kaupp (University of Würzburg) are acknowledged for communicating manuscripts to the authors prior to publication. We thank the Deutsche Forschungsgemeinschaft (DFG Lu 315/13 and Sfb 498, TP C2) and the Fonds der Chemischen Industrie (M.S. and W.L.) for financial support. The Konrad-Zuse-Zentrum für Informationtechnik Berlin (ZIB) is acknowledged for providing a grant of computing time.

References and Notes

(1) Frausto Da Silva, J. J. R.; Williams, R. J. P. *The Biological Chemistry of the Elements: The Inorganic Chemistry of Life;* Clarendon Press: Oxford, UK, 1994.

(2) J. R. Lancaster, J., Ed. *The Bioinorganic Chemistry of Nickel*; VCH: New York, 1988.

(3) Ermler, U.; Grabarse, W.; Shima, S.; Goubeaud, M.; Thauer, R. K. *Curr. Op. Struct. Biol.* **1998**, *8*, 749.

(4) Maroney, M. J.; Davidson, G.; Allan, C. B.; Figlar, J. *Struct. Bonding* **1998**, *92*, 1.

(5) Ragsdale, S. W. *Curr. Op. Chem. Biol.* **1998**, *2*, 208.

(6) Albracht, S. P. J. *Biochim. Biophys. Acta* **1994**, *1188*, 167.

(7) Frey, M. *Struct. Bonding* **1998**, *90*, 97.

(8) Lancaster, J. R., Jr. *Science* **1982**, *216*, 1324.

(9) Huyett, J. E.; Carepo, M.; Pamplona, A.; Franco, R.; Moura, I.; Moura, J. J. G.; Hoffman, B. M. *J. Am. Chem. Soc.* **1997**, *119*, 9291.

(10) Halcrow, M. A.; Christou, G. *Chem. Rev.* **1994**, *94*, 2421.

(11) Volbeda, A.; Charon, M.-H.; Piras, C.; Hatchikian, E. C.; Frey, M.; Fontecilla-Camps, J. C. *Nature* **1995**, *373*, 580.

(12) Higuchi, Y.; Yagi, T.; Yasuoka, N. *Structure* **1997**, *5*, 1671.

(13) Maki, A. H.; Edelstein, N.; Davison, A.; Holm, R. H. *J. Am. Chem. Soc.* **1964**, *86*, 4580.

(14) Schmitt, R. D.; Maki, A. H. *J. Am. Chem. Soc.* **1968**, *90*, 2288.

(15) Huyett, J. E.; Choudhury, S. B.; Eichhorn, D. M.; Bryngelson, P. A.; Maroney, M. J.; Hoffman, B. M. *Inorg. Chem.* **1998**, *37*, 1361.

(16) Sano, M.; Adachi, H.; Yamatera, H. *Bull. Chem. Soc. Jpn.* **1981**, *54*, 2636.

(17) Hayes, R. G. *Inorg. Chem.* **2000**, *39*, 156.

(18) Kraffert, C.; Walther, D.; Peters, K.; Lindqvist, O.; Langer, V.; Sieler, J.; Reinhold, J.; Hoyer, E. *Z. Anorg. Allg. Chem.* **1990**, *588*, 167.

(19) Shiozaki, H.; Nakazumi, H.; Kitao, T. *J. Jpn. Soc. Col. Mater.* **1987**, *60*, 415.

(20) Blomberg, M. A.; Wahlgren, U. *Chem. Phys.* **1980**, *49*, 117−126.

(21) Hjalmars, I. F.; Henrickson-Enflo, A. *Int. J. Quantum Chem.* **1980**, *18*, 409.

(22) Zakharov, I. I.; Startsev, A. N.; Yudanov, I. V.; Zhidomirov, G. M. *J. Struct. Chem.* **1996**, *37*, 201.

(23) Arca, M.; Demartin, F.; Devillanova, F. A.; Garau, A.; Isai, F.; Lelj, F.; Lippols, V.; Pedraglio, S.; Verani, G. *J. Chem. Soc., Dalton Trans.* **1998**, *22*, 3731.

(24) Munzarova, M.; Kaupp, M. *J. Phys. Chem A* **1999**, *103*, 9966.

(25) Morton, J. R.; Preston, K. F. *J. Magn. Res.* **1978**, *30*, 577.

(26) Belanzoni, P.; Baerends, E. J.; van Asselt, S.; Langewen, P. B. *J. Phys. Chem.* **1995**, *99*, 13094.

(27) Belanzoni, P.; Baerends, E. J.; Gribnau, M. *J. Phys. Chem. A* **1999**, *103*, 3732.

(28) Swann, J.; Westmoreland, T. D. *Inorg. Chem.* **1997**, *36*, 5348.

(29) Schreckenbach, G.; Ziegler, T. *J. Phys. Chem. A* **1997**, *101*, 3388.

(30) Schreckenbach, G.; Ziegler, T. *Theor. Chem. Acc.* **1998**, *99*, 71.

(31) Patchkovskii, S.; Ziegler, T. *J. Chem. Phys.* **1999**, *111*(13), 5730.

(32) van Lenthe, E.; Baerends, E. J.; Snijders, J. G. *J. Chem. Phys.* **1993**, *99*, 4597.

(33) van Lenthe, E.; Baerends, E. J.; Snijders, J. G. *J. Chem. Phys.* **1994**, *101*, 9783.

(34) van Lenthe, E.; Wormer, P. E. S.; van der Avoird, A. *J. Chem. Phys.* **1997**, *107*, 2488.

(35) van Lenthe, E.; van der Avoird, A.; Wormer, P. E. S. *J. Chem. Phys.* **1998**, *108*, 4783.

(36) *Amsterdam Density Functional (ADF)*, Rev. 1999; Theoretical Chemistry, Vrije Universiteit: De Boelelaan 1083, NL-1081 HV Amsterdam, The Netherlands.

(37) te Velde, G.; Baerends, E. J. *Int. J. Quantum Chem.* **1992**, *99*, 84.

(38) van Lenthe, E.; Ehlers, A.; Baerends, E. J. *J. Chem. Phys.* **1999**, *110*, 8943.

(39) van Lenthe, E.; Snijders, J. G.; Baerends, E. J. *J. Chem. Phys.* **1996**, *105*, 6505.

(40) Becke, A. D. *J. Chem. Phys.* **1986**, *84*, 4524.

(41) Becke, A. D. *Phys. Rev.* **1988**, *A38*, 3098.

(42) Perdew, J. P. *Phys. Rev.* **1986**, *B33*, 8822.

(43) Perdew, J. P. *Phys. Rev.* **1986**, *B34*, 7406.

(44) Frisch, M. J.; Trucks, G. W.; Schlegel, H. B.; Gill, P. M. W.; Johnson, B. G.; Robb, M. A.; Cheeseman, J. R.; Keith, T.; Petersson, G. A.; Montgomery, J. A.; Raghavachari, K.; Al-Laham, M. A.; Zakrzewski, V. G.; Ortiz, J. V.; Foresman, J. B.; Cioslowski, J.; Stefanov, B. B.; Nanayakkara, A.; Challacombe, M.; Peng, C. Y.; Ayala, P. Y.; Chen, W.; Wong, M. W.; Andres, J. L.; Replogle, E. S.; Gomperts, R.; Martin, R. L.; Fox, D. J.; Binkley, J. S.; Defrees, D. J.; Baker, J.; Stewart, J. P.; Head-Gordon, M.; Gonzalez, C.; Pople, J. A. *Gaussian94*, Revision D.2; Gaussian, Inc.: Pittsburgh, PA, 1995.

(45) Becke, A. D. *J. Chem. Phys.* **1993**, *98*, 5648.

(46) Stevens, P. J.; Devlin, J. F.; Chabalowski, C. F.; Frisch, M. J. *J. Phys. Chem.* **1994**, *98*, 11623.

(47) Barone, V. In *Recent Advances in Density Functional Methods, Part I*; Chong, D. P., Ed.; World Scientific: Singapore, 1995; pp 287−334.

(48) Malkin, V. G.; Malkina, O. L.; Eriksson, L. A.; Salahub, D. R. In *Modern Density Functional Theory: A Tool for Chemistry*; Seminario, J. M., Politzer, P., Eds.; Elsevier: Amsterdam, Netherlands, 1995; pp 273−347.

(49) Eriksson, L. A. In *Encyclopedia of Computational Chemistry*; von Ragué Schleyer, P., Ed.; Wiley and Sons: New York, 1998; pp 952−958.

(50) Kobayashi, A.; Sasaki, Y. *Bull. Chem. Soc. Jpn.* **1977**, *50*, 2650.

(51) Schäfer, A.; Horn, H.; Ahlrichs, R. *J. Chem. Phys.* **1992**, *97*, 2571.

(52) W. E. Geiger, J.; Allen, C. S.; Mines, T. E.; Senftleber, F. C. *Inorg. Chem.* **1977**, *16*, 2003.

(53) Gessner, C.; Stein, M.; Albracht, S. P. J.; Lubitz, W. *J. Biol. Inorg. Chem.* **1999**, *4*, 379.

(54) Assuming that A_{zz} takes the largest value (6 MHz), one has (I) All tensor components positive yields $a_{iso} = +20$ MHz and $A'_{xx,yy,zz} = (+25, -11, -14)$ MHz. (II) $A_{xx,yy,zz} = (+45, +9, -6)$ MHz yields $a_{iso} = +16$ MHz and anisotropic $A'_{xx,yy,zz} = (+29, -7, -22)$ MHz). (III) $A_{xx,yy,zz} = (+45, -9, -6)$ MHz yields $a_{iso} = +10$ MHz, $A'_{xx,yy,zz} = (+35, -19, -16)$ MHz. (IV) $A_{xx,yy,zz} = (+45, -9, +6)$ yields $a_{iso} = +14$ MHz and $A'_{xx,yy,zz} = (+31, -23, -8)$ MHz. The last three possibilities give an isotropic hyperfine interaction in approximate agreement with the liquid solution value. A clear discrimination between the three combinations can be done on the basis of calculations of the (anisotropic) ^{61}Ni hyperfine interaction (see Table 3).

(55) Harriman, J. E. *Theoretical Foundations of Electron Spin Resonance*; Academic Press: New York, 1978.

(56) Atherton, N. M. *Principles of Electron Spin Resonance*; Ellis Horwood PTR Prentice Hall: New York, 1993.

(57) Mabbs, F. E.; Collison, D. *Electron Paramagnetic Resonance of d Transition Metal Compounds*; Elsevier: Amsterdam, Netherlands, 1992.

(58) Abragam, A.; Bleaney, B. *Electron Paramagnetic Resonance of Transition Ions;* Clarendon Press: Oxford, UK, 1970.

(59) Moura, J. J. G.; Moura, I.; Huynh, B. H.; Krüger, H. J.; Texeira, M.; Varney, R. C. D.; DerVartian, D. V.; Xavier, A. V., Jr.; H. D. P.; LeGall, J. *Biochem. Biophys. Res. Commun.* **1982**, *108*, 1388.

(60) Morton, J. R.; Preston, K. F. *J. Chem. Phys.* **1984**, *81*, 5775.

(61) Fan, C.; Teixeira, M.; Moura, J.; Moura, I.; Huynh, B.-H.; Gall, J. L.; Peck, H. D. J.; Hoffman, B. M. *J. Am. Chem. Soc.* **1991**, *113*, 20.

(62) Whitehead, J. P.; Gurbiel, R. J.; Bagyinka, C.; Hoffman, B. M.; Maroney, M. J. *J. Am. Chem. Soc.* **1993**, *115*, 5629.

(63) NR BP86/VTZP calculations with a GTO basis set yielded a_{iso} (^{61}Ni) = +69.85 MHz. The difference between spin-polarized SR ZORA and NR BP86 calculations still lies in the different basis sets (STOs vs GTOs) and/or the consideration of scalar-relativistic effects in the ZORA Hamiltonian.

(64) Trofanchuk, O.; Stein, M.; Gessner, C.; Lendzian, F.; Higuchi, Y.; Lubitz, W. *J. Biol. Inorg. Chem.* **2000**, *5*, 36.